Screening method for producing suitable spray-dried HA powder for SLS application

Henrique Schappo, Karine Giry, Chantal Damia, Dachamir Hotza

Screening Method for Producing Suitable Spray-dried HA powder for SLS application

Henrique Schappo[1,2], Karine Giry[2], Chantal Damia[2], Dachamir Hotza[3]

[1]Innovation Laboratory for Molding and Additive Manufacturing (NIMMA), Federal University of Santa Catarina (UFSC), 88040-900 Florianópolis, SC, Brazil

[2]University of Limoges, CNRS, IRCER, UMR 7315, F-87000 Limoges, France

[3]Interdisciplinary Laboratory for the Development of Nanostructures (LINDEN), Federal University of Santa Catarina (UFSC), 88040-900 Florianópolis, SC, Brazil

Abstract

Screen methods are time-saving tools, assisting the establishment of a new process or technique for laboratory and industrial scale. This paper presents a step-by-step approach to use spray drying (SD) for obtaining hydroxyapatite (HA) powder, with suitable characteristics to be used as a filler in a polymer matrix, for selective laser sintering (SLS) processing. The proposed method consists of adjusting the departing HA suspension and SD processing parameters, briefly discussing relevant elements that must be considered. Suspension's rheological behavior and spray-dried powder morphological features were investigated, serving as selection criteria for the favorable set-up. Variations on slurry feed and atomization pressure of SD processing parameters have allowed obtaining different powder characteristics. A major influence of atomization pressure variation was identified, a greater pressure value resulted in smaller particle size. Desirability function was employed to determine the optimal SD processing parameters, in other words, conditions that made it possible to obtain spherical particles with the proposed mean diameter in the range of 15 to 25 µm, with narrow particle size distribution.

Keywords: spray drying, hydroxyapatite, selective laser sintering, tissue engineering.

1. Introduction

Customized fabricated parts are required in a wide range of applications, being particularly important in medicine. The feasibility of manufacturing complex geometries, combining different materials, matches with the requirements of implantable devices used for human tissue recovery. Tissue engineering (TE) seeks to restore, maintain, or improve damaged tissues through the combination of scaffolds, cells, and biologically active molecules into functional tissues [1].

Human bone is a complex vascularized structure, composed of organic collagen fibrils and inorganic calcium phosphate (CaP) crystals [2]. CaP materials [3,4] such as hydroxyapatite (HA) and beta-tricalcium phosphate (β-TCP) are widely used as bone substitutes and are commercially found in a few different geometries (e.g. granules and sticks). However, the fabrication of customized scaffolds from these materials remains a challenge, especially in terms of patient's implant fitting. Additive manufacturing (AM) is a breakthrough technology that allowed significant progress for tissue engineering applications, and still reveals promising solutions for custom-made bone scaffolds [5–8].

Powder bed fusion, frequently referred to as selective laser sintering (SLS) is one of the commercially available AM processes [9]. In this process, particulate materials are fused layer by layer via heat supplied by an infrared laser source, creating 3D parts that were originally designed using computer-assisted design (CAD) tools. SLS does not need any support during manufacturing and presents high resolution and fast processing. On the other hand, SLS is carried out at high processing temperatures and the manufactured parts are characterized by a rough surface finish [10]. Nevertheless, SLS can be considered one of the most versatile AM techniques in terms of material usage and structural stability. Moreover, through optimized parameters, it is possible to achieve the desired mechanical properties for TE scaffolds [11]. SLS processing with proper materials selection can contribute to enhancing the scaffold's final properties, particularly bioactivity [12,13]. When processing composite materials (*i.e.* bioceramic fillers in a polymeric matrix) a substantial difference between material's particle size is beneficial, allowing the filler to occupy voids in the interstices of matrix particles. Concerning polymer SLS feedstock, there are preferable powder

characteristics that improve the sinterability and final properties of the fabricated piece [14,15]. Related literature has indicated better processing and geometry accuracy when using spherical particles and narrow particle size distribution with an average size below 150 μm or equivalent to the laser beam diameter [14,16]. Spherical HA particles can be obtained by different techniques [17–23] in a diverse range of particle sizes. However, process scalability remains a challenge and not all techniques are capable of producing particles in the range of 15 to 25 μm.

Spray drying (SD) consists of the transformation of a fluid material into dried particles. SD had shown remarkable development in the last decades, being used by different industries [24]. SD commercial equipment may differ in terms of configuration. Rotary, hydraulic and pneumatic nozzle atomizers are commonly used [15]. The variables that affect how the spray is mixed with the hot gas depend upon the type of gas flow: co-current, countercurrent, or mixed flow [25]. Spray-dried HA (SDHA) powder has been successfully employed for distinct biomedical applications, using different manufacturing techniques [26–31]. Moreover, SD enables advantageous powder characteristics that are desirable for 3D printing use [24]. Although SDHA powder morphology indicates suitability for SLS processing, publications concerning this subject are scarce [32]. Similarly, comprehensive information about how to produce SDHA powders for SLS processing is rarely reported in the literature. This paper proposes a screening method for producing suitable HA powders for SLS processing.

2. Materials and methods

2.1. Materials and compositions

Suspensions to be spray-dried were prepared with nano-sized HA [$Ca_{10}(PO_4)_6(OH)_2$] synthesized in-house by hydrothermal route. Synthesis further details can be found elsewhere [33]. Methylcellulose (Methocel A15 Premium LV, Dow Chemical) was added as a binder to form an aqueous suspension using deionized water, according to the compositions in Table 1.

Table 1 – Compositions of spray-drying HA aqueous suspensions.

2.2. Spray drying parameters

A mini spray drying machine (Buchi B-290) was used. As displayed in Figure 1, the slurry mixture is pumped through a pneumatic external mixing nozzle (2) and sprayed by the spray gas (1) into the drying chamber (4). The drying gas (3) is heated and serves as a carrier for the spray-dried particles that will be deposited in the recipient (5) under the cyclone (6). Larger particles that were not carried by the drying gas can be recuperated under the drying chamber. Smaller particles will be retained in the filter (7).

Some spray drying parameters were kept constant in all experiments: inlet temperature of hot air 170 °C, volume flow of hot air aspiration 39 $m^3\ h^{-1}$, slurry feed 21 $mL.min^{-1,}$ and atomization flow 45 mmHg.

Figure 1 – Scheme of BUCHI B-290 mini spray drying [34].

A pneumatic nozzle with 2.00 mm diameter was used. It is possible to rotate the nozzle cap in order to get different widths of the spraying cone. Nozzle circumference of 8.5 mm was divided in 5 positions: 0, I, II, III, IV, whereas position 0 was only used as a point of referent (nozzle cap tightest position). Each position represents a different width of the cone spray produced by the nozzle, being position I the widest cone spray.

The intention is to use spray dried HA particles as a filler in a polymeric matrix. In this sense, better homogeneity and cohesion within materials can be achieved when HA particles are smaller and can be located in the voids of polymeric particles. Therefore, to obtain spherical HA particles, possessing an average diameter of 15 to 25 µm and narrow particle size distribution, two SD parameters were varied slurry feed and atomization pressure. A factorial design experiment with two factors and two levels was carried out (Table 3). The optimal point among the experimental results originated from factorial design

was determined using a desirability function. Results were ranked by preferable attributes taking into consideration the D50 value, (D90-D10)/D50 and particle morphology.

2.3. Characterization of powder and suspension

Morphological analysis was performed using a scanning electron microscope (SEM, JEOL IT300LV), after coating the samples with platinum (Agar Scientific). Departure HA powder was analyzed, without coating, using a field emission gun microscope (FEI, Quanta 450). Particle size and distribution (PSD) were determined by a laser scattering (Partica LA-950V2, Horiba). The specific surface area was measured by nitrogen adsorption (ASAP 2020, Micromeritics) and calculated according to the Brunauer–Emmet–Teller equation. X-ray diffraction (XRD, D8 Advance, Bruker) was carried out with a scan range from 27° to 40°, 2θ of 0.02° and acquisition time of 5 s. For XRD phase identification, EVA software was employed using HA's diffraction pattern (Powder Diffraction Files – PDF: 00-09-0432) from International Center for Diffraction Data (ICDD). The rheological behavior of HA slurries was assessed with a concentric rheometer (AR1500 TA Instruments, US) using a 40 mm parallel plate. Rheology flow sweep measurements were performed on suspensions 20 °C, namely 10 points over stress rates from 0.1 to 40 Pa. The Herschel–Bulkley model was fitted to experimental data. After spray drying, the sprayed powder was submitted to thermal treatment using ramps of 3 °C/min up to 500 °C, for binder removal, and 10 °C/min up to 1000 °C, with a hold at this temperature for 1 h, for densification (LHT 04/17, Nabertherm GmbH).

3. Results and discussion

3.1. Raw powder characteristics

The synthesized HA powder had a specific surface area of around 80 $m^2\ g^{-1}$. As a means to reduce its reactivity, the powder was heat-treated at 650 °C for 30 min resulting in a surface area of 34 $m^2\ g^{-1}$. This heat treatment allows eliminating synthesis residues (*i.e.* nitrate and ammonium ions), providing a

homogeneous specific surface and reproducible characteristics of the departing powder. Further, it contributes to a more stable suspension and minimizing agglomeration between HA particles. Heat treatment and SD processing did not affect the phase compositions, being the same of pure HA according to diffraction pattern (Figure 2). As revealed on SEM images (Figure 3) and PSD curve (Figure 4) the nano-sized HA particles (D50 value 0.13 μm) have a tendency to agglomerate, therefore, the suspension for SD processing must be carefully prepared.

Figure 2 – XRD curves of pure HA treated at 650 °C for 0.5 h and SDHA treated at 1000 °C for 1 h.

Figure 3 – SEM-FEG images of heat-treated departing HA powder, indicating the tendency of the agglomeration (left). Close-up of agglomerated nano-sized particles (right).

Figure 4 – PSD curve of heat-treated departing HA powder.

3.2. Effect of suspension formulation

Suspension composition has major importance because its characteristics will influence all the spray drying process. For this step, the trial and error experimentation method is applicable when no information is found in the literature. However, there are aspects of fundamental importance to be considered (*e.g.* maximal solid content, slurry viscosity) that can be easily found in the related bibliography. Moreover, machine manufacturers can provide elementary information about recommended processing characteristics. Early trial and error experiments, together with literature information, have provided a point of departure in terms of mixture preparation, solid content, binder selection, and processing parameter values.

First, the binder selection must consider the powder's final application (in this case, bone tissue applications). Therefore, after processing, it must maintain the original HA chemical composition. In previous essays, the performance of different binders: corn starch (Roquette, ref: 764071), polyvinylpyrrolidone (grade 30 and 90 from BASF), and methylcellulose (Methocel A15-LV Premium) were analyzed. Methylcellulose demonstrated a larger average particle size, better process efficiency, and requiring lower concentrations. Spray-dried HA (SDHA) powder, after heat treatment at 1000 °C for 1 h, has matching phase compositions to heat-treated HA as shown in Figure 2, confirming the suitability of methylcellulose in terms of not modifying powder composition.

Once the type of binder is selected, the amount of HA must be defined. Adding too much HA in the suspension will prevent good homogeneity and induce solid deposition. Moreover, it will increase viscosity and difficult spray drying processing (i.e. nozzle blocking). On the other hand, a low solid concentration will result in a smaller particle size [35]. Previous essays indicated the use of around 20 wt% HA content for the proposed screening method and particle size objectives. To guarantee suspension homogeneity, it is recommended to agitate with a magnetic stirrer for at least 10 h before starting the spray drying process. While processing, continuously stirring is required to maintain the mixture uniform and with constant viscosity [36].

SD process is highly dependent on the suspension's characteristics and its viscosity has a great influence on the obtained powder. As detailed in Figure 5, the amount of methylcellulose has a large effect on the suspension's rheology. Table 2 provides the values obtained from the slurry rheological analysis, Herschel–Bulkley model was used given its fitting with experimental results. Yield stress values were similar between SD01-SD02 and SD03-SD04, indicating two types of behavior according to binder amount. All the suspensions showed pseudoplastic shears thinning behavior, implicating in a viscosity decrease with increasing shear rate. This is an important characteristic that guarantees suspension uniform viscosity along with all the SD processing, under constant agitation. Large viscous forces will need more energy for breaking the droplets, resulting in larger droplets [37]. This phenomenon was observed when processing SD01, where occurred slurry droplets deposition in the drying chamber.

PSD analyses were performed for all suspensions (Figure 6). Although the suspensions have similar dispersion curves, SD01 and SD02 indicate a larger volume of particles around 50 µm area, suggesting that the suspension is not well homogenized. As detailed in Table 2, this bimodal distribution reflects the values of D10, D50, D90, and its ratio. Particle size values of D10 mean that 10% of particles have smaller diameters than the D10 value, in the same way, D50 and D90 represent the 50% and 90% portions. (D90-D10)/D50 ratio provides information related to the particles' distribution width, in which, a wider distribution is observed with high ratio values. The values obtained by (D90-D10)/D50 ratio enhance the significant distribution behavior of SD01-SD02 versus SD03-SD04. It is possible that suspensions SD01 and SD02 have not completely dissolved the binder, remaining agglomerates. Individual nano-sized HA particles tend to gather together (Figure 3), accentuating agglomeration effects.

SEM images (Figure 7) suggest that the high amount of methylcellulose binder in suspensions SD01 and SD02 formed binder agglomerates in the particles, causing defects after sintering that can be observed by the empty spaces in the particles (forming donut-like particles). Contrastingly, heat-treated SD04 powder presented some particles with an insufficient amount of binder, preventing proper cohesion between HA departing particles (also evidenced by smaller values on PSD) and restricting the formation of appropriate morphology.

According to rheological analysis and PSD values, SD03 and SD04 have shown the most suitable results. When also considering morphological characteristics of spray-dried granules, SD04 did not have a sufficient amount of binder to guarantee proper cohesion of nano-sized HA particles, therefore, SD03 was chosen to proceed with the following steps.

Figure 5 – Viscosity measurements of HA suspensions SD01, SD02, SD03, and SD04.

Figure 6 – PSD curves of suspensions SD01, SD02, SD03, and SD04.

Table 2 – Rheological values obtained from the Herschel–Bulkley model and respective D10, D50, D90, and ratio measures for HA suspensions.

Figure 7 – SEM images of HA particles from SD01, SD02, SD03, and SD04, after heat treatment at 1000 °C for 1 h.

3.3. Effect of spray drying parameters

Nozzle cap position is important to avoid excessive droplets deposition on the drying chamber wall, which can result in lower process efficiency. In order to verify any influence of spray width on the particle's morphology, particle measurement and SEM images were conducted. Particle size distribution (Figure 8) and morphology have shown to be similar between the nozzle's four positions (SD05 to SD08), hence, these attributes were not directly affected by the changes in the spray angles, neither they were sufficient to validate an optimal nozzle position.

Considering the similarity in morphology and particle size distribution, position II was chosen because SD06 had around 5% more process yield (powder recover quantity) when compared to the others.

Figure 8 – PSD of HA densified particles (after heat treatment at 1000 °C for 1 h): SD05 (pos. I), SD06 (pos. II), SD07 (pos. III), SD08 (pos. IV).

The final properties of spray-dried particles are highly dependent on processing parameters, as well as equipment's features and configurations. Although it is possible to adjust particle characteristics by changing the processing parameters, it is necessary to establish a suitable departing suspension to achieve

the targeted goals in terms of particle. Afterward, the heat treatment process will affect the particle density, crystallinity, and mechanical integrity [38]. Considering that heat treatment is a post-process of spray drying, not directly influencing the particle size distribution and morphology, it will not be investigated here. In terms of particle-size distribution and process yield, key parameters are suspension's solid content, spray drying slurry feed, and atomization pressure; yet, other factors like nozzle diameter, inlet temperature, aspirator velocity, and drying gas humidity also influence the obtained particles [25,38,39]. As mentioned before, an early trial and error method should be applied to comprehend the basic correlations between all the processing factors. In-depth analysis for investigating the influence of different processing variables should be done using statistical tools and it is recommended to perform at least 3 replicates for establishing any conclusions.

Table 3 – Factorial design parameters and values and respective D10, D50, D90 mean size and size ratios, after heat treatment at 1000 °C for 1 h. The (-) signal represents lower and (+) higher values of the two levels factorial design.

Particle size information is displayed in Figure 8 and Table 3. It has been reported in the related bibliography that a higher atomization pressure decreases the particle size [35,38,40]. This observation is in accordance with our results, when comparing SD09 and SD11 (same slurry feed and SD11 with higher atomization pressure), SD11 possesses lower particle values for D10 and D50. In the same manner, SD12 has D10, D50, and D90 particle size lower than SD10 (same slurry feed and SD12 with higher atomization pressure). On the other hand, from our results, it was not possible to observe the association between larger particle sizes with increases in slurry feed rate reported in the literature [38,40]. Analyzing the curves in Figure 9, it can be observed similarities between SD09-SD10 and SD11-SD12, this might indicate a minor influence of slurry feed in our experiences. Probably, a greater difference between slurry feed values would evidence variances in particle size. Nevertheless, it is important to highlight that these comparisons

are only illustrative, for representative conclusions it would be necessary more replicates, experimental error determination, and the use of statistical analysis of variance (ANOVA). SEM images (Figure 10) have shown similar spherical morphology for the respecting spray-dried powder and, as expected, a greater population of bigger particles were observed on SD09 and SD10.

Figure 9 – PSD dispersions of HA particles SD09, SD10, SD11, SD12, after heat treatment at 1000 °C for 1 h.

Figure 10 – SEM images of HA particles SD09, SD10, SD11, and SD12, heat-treated at 1000 °C for 1 h.

Introducing satisfaction index for the responses D50, (D90-D10)/D50 and particle morphology, desirability values were obtained (Table 4). Individual desirability of D50 and morphology were calculated using $\mathcal{D} = (Yi - L)/(T - L)$ equation, where Yi is the response, L the lower value, and T the target value. Conversely, for (D90-D10)/D50 desirability a minimized result was targeted, therefore, $\mathcal{D} = (U - Yi)/(U - T)$ equation was used (U means upper value). The applied ranges of values were: i) D50: 100% desirability if value greater than 25 and 0% desirability if value less than 15; ii) (D90-D10)/D50: 100% desirability if value less than 1 and 0% desirability if value greater than 3; iii) particle morphology: 100% desirability if value greater than 5, 0% desirability if value less than 1. For particle morphology, SEM images were analyzed and for each sample, it was given a 1 to 5 score (5 is the most suitable morphology). Higher values of desirability were observed on SD09 and SD10 mainly due to D50 and (D90-D10)/D50.

Although global desirability pointed out SD09 and SD10 as the most suitable powder characteristics, all SD powders achieved the proposed morphology and size objectives. The variation of two processing parameters has shown the capability of adjusting particle size characteristics.

Table 4 – Samples and respective desirability responses.

4. Conclusions

This screening method contemplates the main steps for powder preparation suitable for SLS. Spray-dried HA particles were successfully produced within the proposed morphology. Binder and HA content of the departing slurry have an important effect on viscosity. Therefore, special attention must be given to preparing the departing suspension. Variations on spray drying processing parameters have shown the possibility of tailoring particle size and distribution. For a proper analysis of the processing parameters variation, statistical tools must be used. PSD and SEM images have indicated suitable particle characteristics for SLS processing, although additional studies must be conducted to confirm SLS processability. The versatility of the proposed method makes it possible to be applied in other bioceramic materials and types of binders, targeting different particle sizes.

Acknowledgments

This study was financed in part by Coordenação de Aperfeiçoamento de Pessoal de Nível Superior – Brasil (CAPES) - Finance Code 001, and Fundação de Amparo à Pesquisa e Inovação do Estado de Santa Catarina (FAPESC). The authors thank the French Agence Nationale de la Recherche in the scope of the LabExSigmaLim (ANR-10-LABX-0074-01 Sigma-LIM). The authors are grateful to the Service Commun de Caractérisation des Matériaux de Limoges (CARMALIM) and more especially to Yann Launay for SEM acquisitions, Marguerite Bienia and Mickäel Lacroix for rheological measurements. The authors also thank Emeline Renaudie for her assistance in the elaboration of calcium phosphate ceramics, and Geoffroy Rivaud for the support in spray drying.

References

[1] R. Langer, J. Vacanti, Tissue engineering, Science (80-.). 260 (1993) 920–926.

https://doi.org/10.1126/science.8493529.

[2] L. Piaia, G.V. Salmoria, D. Hotza, Additive manufacturing of nanostructured bone scaffolds, Elsevier Inc., 2018. https://doi.org/10.1016/B978-0-12-814621-7.00010-X.

[3] J.C. Elliott, Structure and chemistry of the apatites and other calcium orthophosphates, Elsevier, 2013.

[4] L.L. Hench, Bioceramics, J. Am. Ceram. Soc. 81 (1998) 1705–1728. https://doi.org/10.1111/j.1151-2916.1998.tb02540.x.

[5] L. Piaia, G.V. Salmoria, D. Hotza, Additive Manufactured Nanocomposites for Bone Tissue Engineering Applications: an Overview, Mater. Res. 23 (2020) 1–10. https://doi.org/10.1590/1980-5373-mr-2019-0487.

[6] S. Mondal, U. Pal, 3D hydroxyapatite scaffold for bone regeneration and local drug delivery applications, J. Drug Deliv. Sci. Technol. 53 (2019) 101131. https://doi.org/10.1016/j.jddst.2019.101131.

[7] J. D'Alessio, A. Christensen, 3D Printing for Commercial Orthopedic Applications: Advances and Challenges, in: 3D Print. Orthop. Surg., Elsevier, 2019: pp. 65–83. https://doi.org/10.1016/B978-0-323-58118-9.00007-5.

[8] C. Shuai, L. Yu, W. Yang, S. Peng, Y. Zhong, P. Feng, Phosphonic acid coupling agent modification of HAP nanoparticles: Interfacial effects in PLLA/HAP bone scaffold, Polymers (Basel). 12 (2020). https://doi.org/10.3390/polym12010199.

[9] ISO/ASTM 52900: 2015 Additive manufacturing-General principles-terminology, ASTM F2792-10e1. (2012).

[10] G.-H. Wu, S. Hsu, Review: polymeric-based 3D printing for tissue engineering, J. Med. Biol. Eng. 35 (2015) 285–292.

[11] F.E. Wiria, K.F. Leong, C.K. Chua, Y. Liu, Poly-ε-caprolactone/hydroxyapatite for tissue engineering scaffold fabrication via selective laser sintering, Acta Biomater. 3 (2007) 1–12. https://doi.org/10.1016/j.actbio.2006.07.008.

[12] C. Shuai, W. Yang, P. Feng, S. Peng, H. Pan, Accelerated degradation of HAP/PLLA bone scaffold by PGA blending facilitates bioactivity and osteoconductivity, Bioact. Mater. 6 (2021) 490–502. https://doi.org/10.1016/j.bioactmat.2020.09.001.

[13] P. Feng, S. Peng, C. Shuai, C. Gao, W. Yang, S. Bin, A. Min, In Situ Generation of Hydroxyapatite on Biopolymer

316 Particles for Fabrication of Bone Scaffolds Owning Bioactivity, ACS Appl. Mater. Interfaces. 12 (2020) 46743–
317 46755. https://doi.org/10.1021/acsami.0c13768.

318 [14] M. Schmid, A. Amado, K. Wegener, Materials perspective of polymers for additive manufacturing with
319 selective laser sintering, J. Mater. Res. 29 (2014) 1824–1832. https://doi.org/10.1557/jmr.2014.138.

320 [15] D. Sofia, D. Barletta, M. Poletto, Laser sintering process of ceramic powders: The effect of particle size on the
321 mechanical properties of sintered layers, Addit. Manuf. 23 (2018) 215–224.
322 https://doi.org/10.1016/j.addma.2018.08.012.

323 [16] R.D. Goodridge, C.J. Tuck, R.J.M. Hague, Laser sintering of polyamides and other polymers, Prog. Mater. Sci.
324 57 (2012) 229–267. https://doi.org/10.1016/j.pmatsci.2011.04.001.

325 [17] C. Li, G. Li, S. Liu, J. bai, A. zhang, Spherical hydroxyapatite with colloidal stability prepared in aqueous
326 solutions containing polymer/surfactant pair, Colloids Surfaces A Physicochem. Eng. Asp. 366 (2010) 27–33.
327 https://doi.org/10.1016/j.colsurfa.2010.05.018.

328 [18] G.C. Koumoulidis, A.P. Katsoulidis, A.K. Ladavos, P.J. Pomonis, C.C. Trapalis, A.T. Sdoukos, T.C. Vaimakis,
329 Preparation of hydroxyapatite via microemulsion route, J. Colloid Interface Sci. 259 (2003) 254–260.
330 https://doi.org/10.1016/S0021-9797(02)00233-3.

331 [19] K. Ioku, G. Kawachi, S. Sasaki, H. Fujimori, S. Goto, Hydrothermal preparation of tailored hydroxyapatite, J.
332 Mater. Sci. 41 (2006) 1341–1344. https://doi.org/10.1007/s10853-006-7338-5.

333 [20] C. Qiu, X. Xiao, R. Liu, Biomimetic synthesis of spherical nano-hydroxyapatite in the presence of polyethylene
334 glycol, Ceram. Int. 34 (2008) 1747–1751. https://doi.org/10.1016/j.ceramint.2007.06.001.

335 [21] M.H. Hong, J.S. Son, K.M. Kim, M. Han, D.S. Oh, Y.K. Lee, Drug-loaded porous spherical hydroxyapatite
336 granules for bone regeneration, J. Mater. Sci. Mater. Med. 22 (2011) 349–355.
337 https://doi.org/10.1007/s10856-010-4197-z.

338 [22] X. Ma, Y. Chen, J. Qian, Y. Yuan, C. Liu, Controllable synthesis of spherical hydroxyapatite nanoparticles using
339 inverse microemulsion method, Mater. Chem. Phys. 183 (2016) 220–229.
340 https://doi.org/10.1016/j.matchemphys.2016.08.021.

341 [23] M. Kamitakahara, S. Takahashi, T. Yokoi, C. Inoue, K. Ioku, Preparation of spherical porous hydroxyapatite

granules as support materials for microorganisms, J. Ceram. Soc. Japan. 126 (2018) 732–735. https://doi.org/10.2109/jcersj2.18089.

[24] D. Santos, A.C. Maurício, V. Sencadas, J.D. Santos, M.H. Fernandes, P.S. Gomes, Spray Drying: An Overview, in: Biomater. - Phys. Chem. - New Ed., InTech, 2018. https://doi.org/10.5772/intechopen.72247.

[25] K. Cal, K. Sollohub, Spray Drying Technique. I: Hardware and Process Parameters, J. Pharm. Sci. 99 (2010) 575–586. https://doi.org/10.1002/jps.21886.

[26] Y.J. Fu, S.S. Shyu, F.H. Su, P.C. Yu, Development of biodegradable co-poly(D, L-lactic/glycolic acid) microspheres for the controlled release of 5-FU by the spray drying method, Colloids Surfaces B Biointerfaces. 25 (2002) 269–279. https://doi.org/10.1016/S0927-7765(01)00205-3.

[27] P. López-Gasco, I. Iglesias, J. Benedí, R. Lozano, J.M. Teijón, M.D. Blanco, Paclitaxel-loaded polyester nanoparticles prepared by spray-drying technology: In vitro bioactivity evaluation, J. Microencapsul. 28 (2011) 417–429. https://doi.org/10.3109/02652048.2011.576785.

[28] E. Quinlan, A. López-Noriega, E.M. Thompson, A. Hibbitts, S.A. Cryan, F.J. O'Brien, Controlled release of vascular endothelial growth factor from spray-dried alginate microparticles in collagen–hydroxyapatite scaffolds for promoting vascularization and bone repair, J. Tissue Eng. Regen. Med. 11 (2017) 1097–1109. https://doi.org/10.1002/term.2013.

[29] S. Sequeira, M.H. Fernandes, N. Neves, M.M. Almeida, Development and characterization of zirconia–alumina composites for orthopedic implants, Ceram. Int. 43 (2017) 693–703. https://doi.org/10.1016/j.ceramint.2016.09.216.

[30] Y. Ben, L. Zhang, S. Wei, T. Zhou, Z. Li, H. Yang, Y. Wang, F.A. Selim, C. Wong, H. Chen, PVB modified spherical granules of β-TCP by spray drying for 3D ceramic printing, J. Alloys Compd. 721 (2017) 312–319. https://doi.org/10.1016/j.jallcom.2017.06.022.

[31] R. Cholas, S. Kunjalukkal Padmanabhan, F. Gervaso, G. Udayan, G. Monaco, A. Sannino, A. Licciulli, Scaffolds for bone regeneration made of hydroxyapatite microspheres in a collagen matrix, Mater. Sci. Eng. C. 63 (2016) 499–505. https://doi.org/10.1016/j.msec.2016.03.022.

[32] C.K. Chua, K.F. Leong, K.H. Tan, F.E. Wiria, C.M. Cheah, Development of tissue scaffolds using selective laser

368 sintering of polyvinyl alcohol/hydroxyapatite biocomposite for craniofacial and joint defects, J. Mater. Sci.
369 Mater. Med. 15 (2004) 1113–1121. https://doi.org/10.1023/B:JMSM.0000046393.81449.a5.

370 [33] S. Raynaud, E. Champion, D. Bernache-Assollant, P. Thomas, Calcium phosphate apatites with variable Ca/P
371 atomic ratio I. Synthesis, characterisation and thermal stability of powders, Biomaterials. 23 (2002) 1065–
372 1072. https://doi.org/10.1016/S0142-9612(01)00218-6.

373 [34] Büchi Labortechnik AG, Mini Spray Dryer B-290: Product Brochure, (2020).

374 [35] A.J. Wang, Y.P. Lu, R.F. Zhu, S.T. Li, X.L. Ma, Effect of process parameters on the performance of spray-dried
375 hydroxyapatite microspheres, Powder Technol. 191 (2009) 1–6.
376 https://doi.org/10.1016/j.powtec.2008.10.020.

377 [36] Q. Murtaza, J. Stokes, M. Ardhaoui, Experimental analysis of spray dryer used in hydroxyapatite thermal spray
378 powder, J. Therm. Spray Technol. 21 (2012) 963–974. https://doi.org/10.1007/s11666-012-9791-9.

379 [37] S.P. Anandharamakrishnan, C.; Ishwarya, Spray Drying Techniques for Food Ingredient Encapsulation, John
380 Wiley & Sons, 2015.

381 [38] F.E. Bastan, G. Erdogan, T. Moskalewicz, F. Ustel, Spray drying of hydroxyapatite powders: The effect of spray
382 drying parameters and heat treatment on the particle size and morphology, J. Alloys Compd. 724 (2017) 586–
383 596. https://doi.org/10.1016/j.jallcom.2017.07.116.

384 [39] Büchi Labortechnik AG, Process parameters Spray drying, 2020. https://www.buchi.com/en/products/spray-
385 drying-and-encapsulation/mini-spray-dryer-b-290.

386 [40] P. Luo, T.G. Nieh, Preparing hydroxyapatite powders with controlled morphology, Biomaterials. 17 (1996)
387 1959–1964. https://doi.org/10.1016/0142-9612(96)00019-1.

388

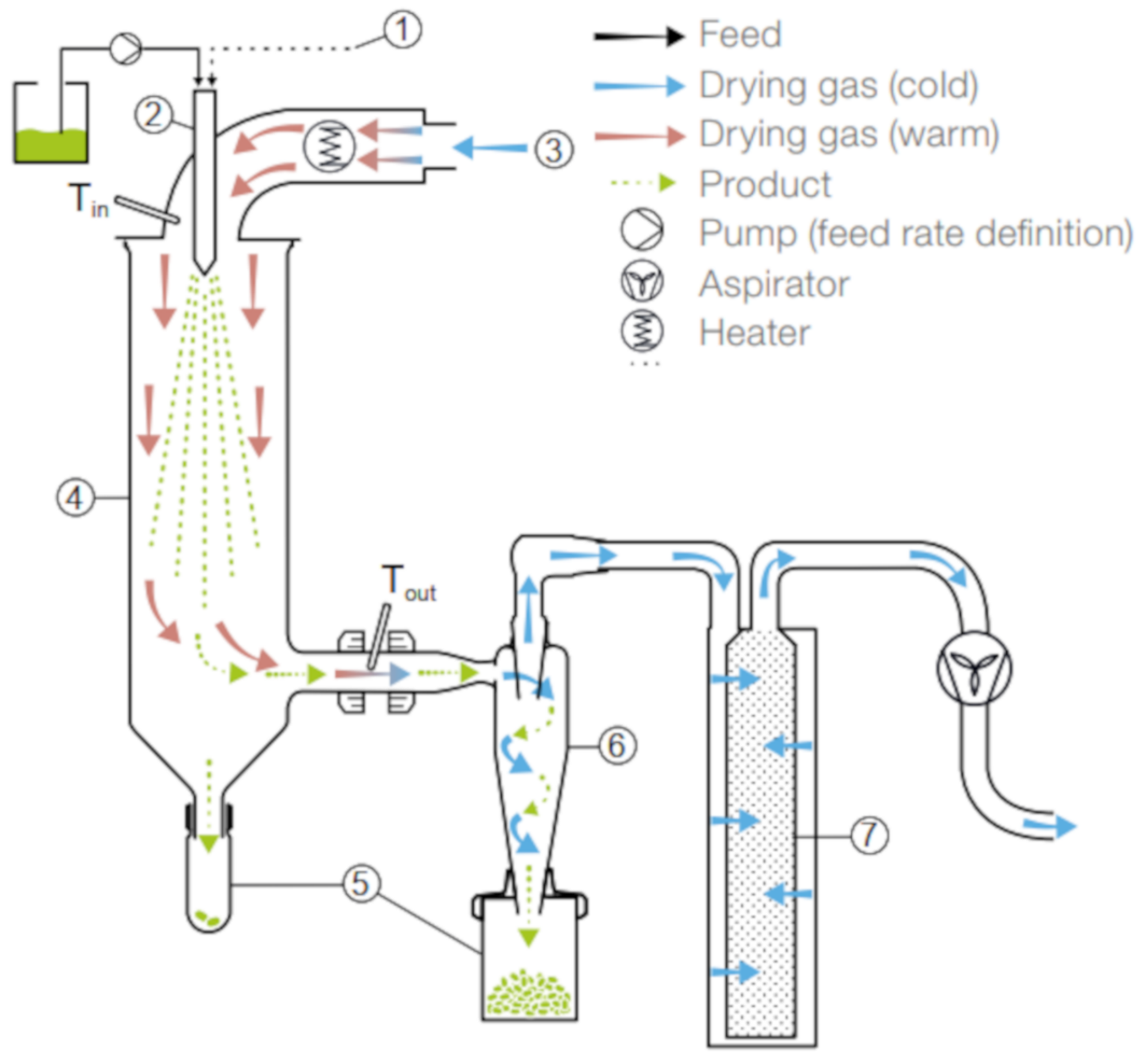
1
2
3
4
5
6
7
T_{in}
T_{out}
Feed
Drying gas (cold)
Drying gas (warm)
Product
Pump (feed rate definition)
Aspirator
Heater

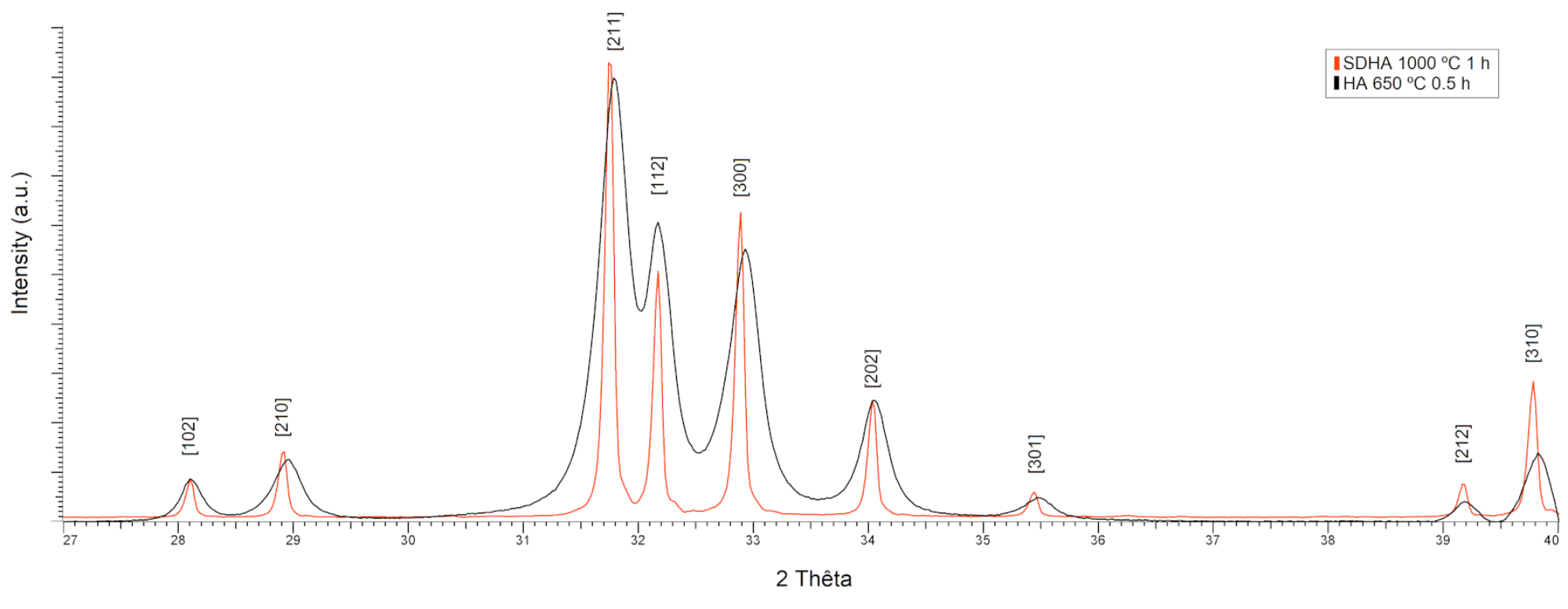
SDHA 1000 °C 1 h
HA 650 °C 0.5 h
Intensity (a.u.)
2 Thêta
[102]
[210]
[211]
[112]
[300]
[202]
[301]
[212]
[310]
27
28
29
30
31
32
33
34
35
36
37
38
39
40

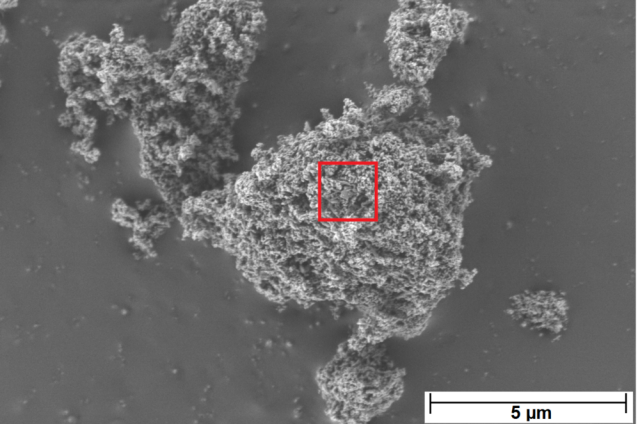
5 µm

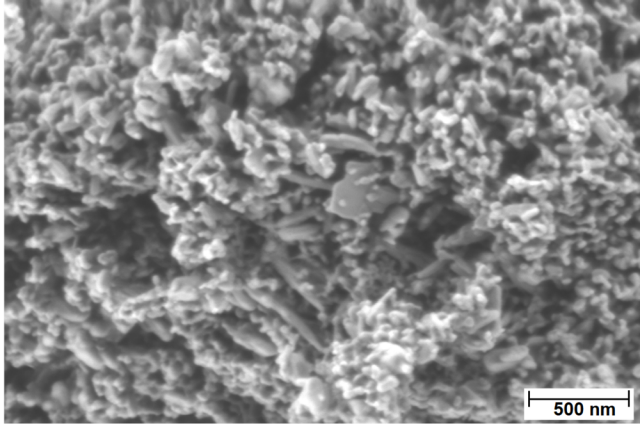
500 nm


Counts
Channel (ch)

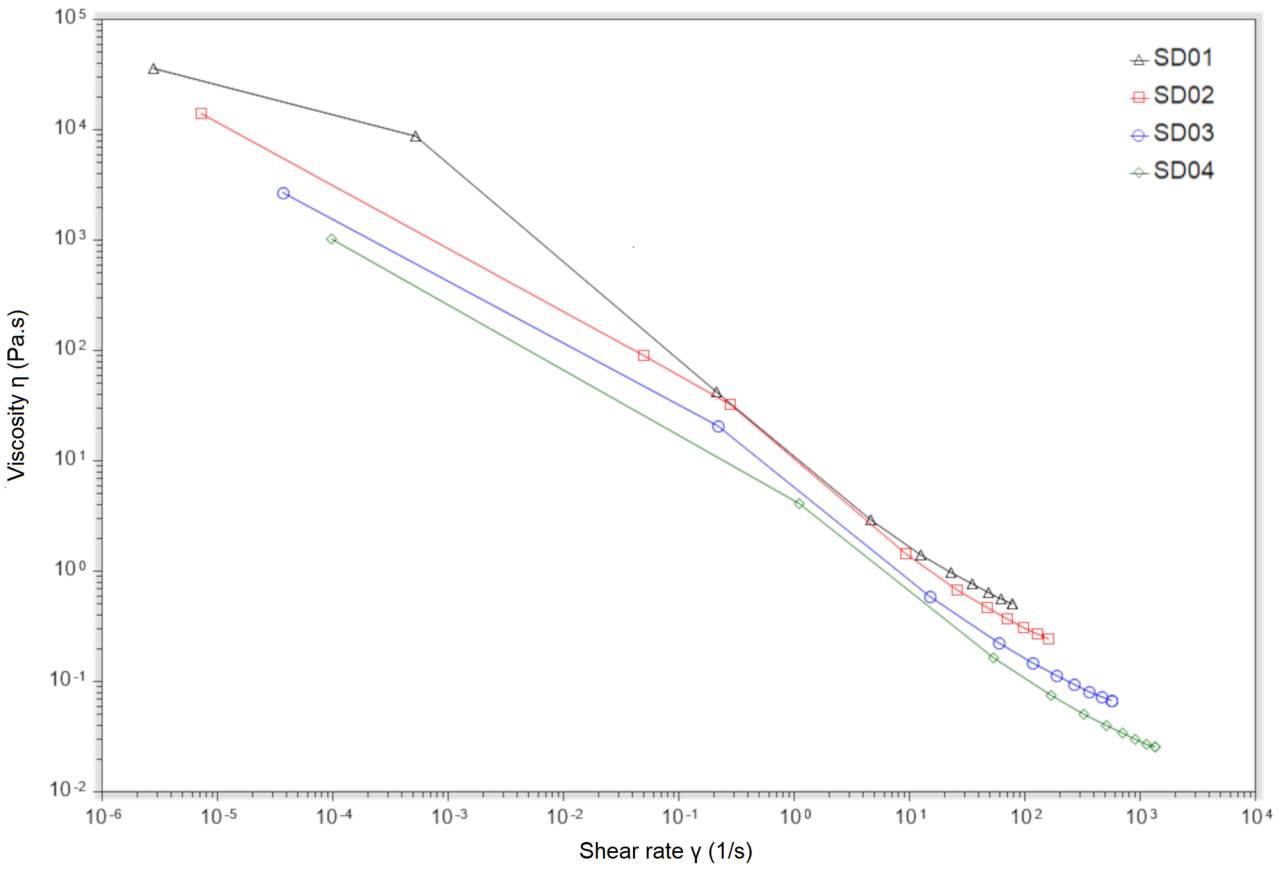
SD01
SD02
SD03
SD04
Viscosity η (Pa.s)
Shear rate γ (1/s)
10⁵
10⁴
10³
10²
10¹
10⁰
10⁻¹
10⁻²
10⁻⁶
10⁻⁵
10⁻⁴
10⁻³
10⁻²
10⁻¹
10⁰
10¹
10²
10³
10⁴

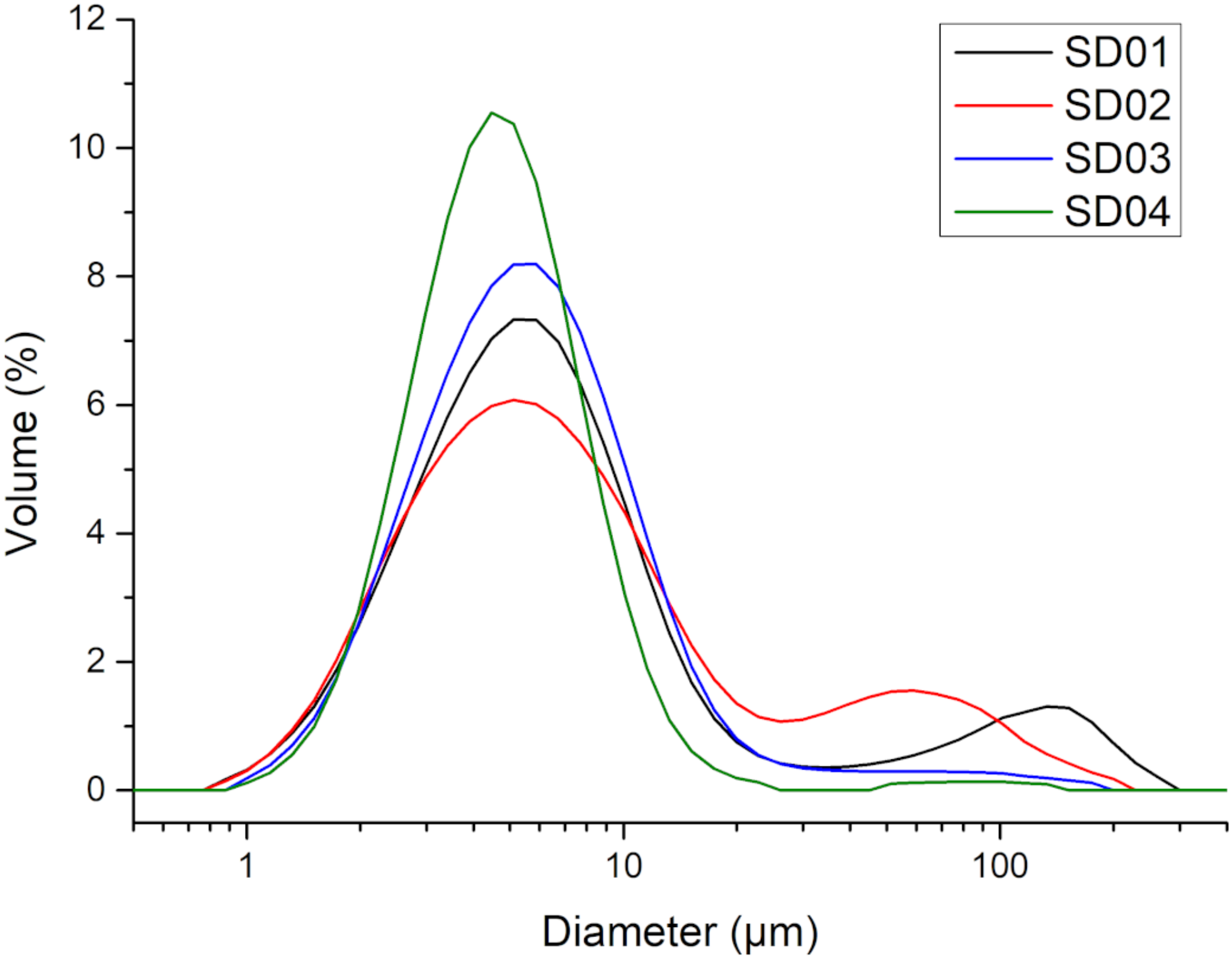
SD01
SD02
SD03
SD04
Volume (%)
Diameter (μm)
0
2
4
6
8
10
12
1
10
100

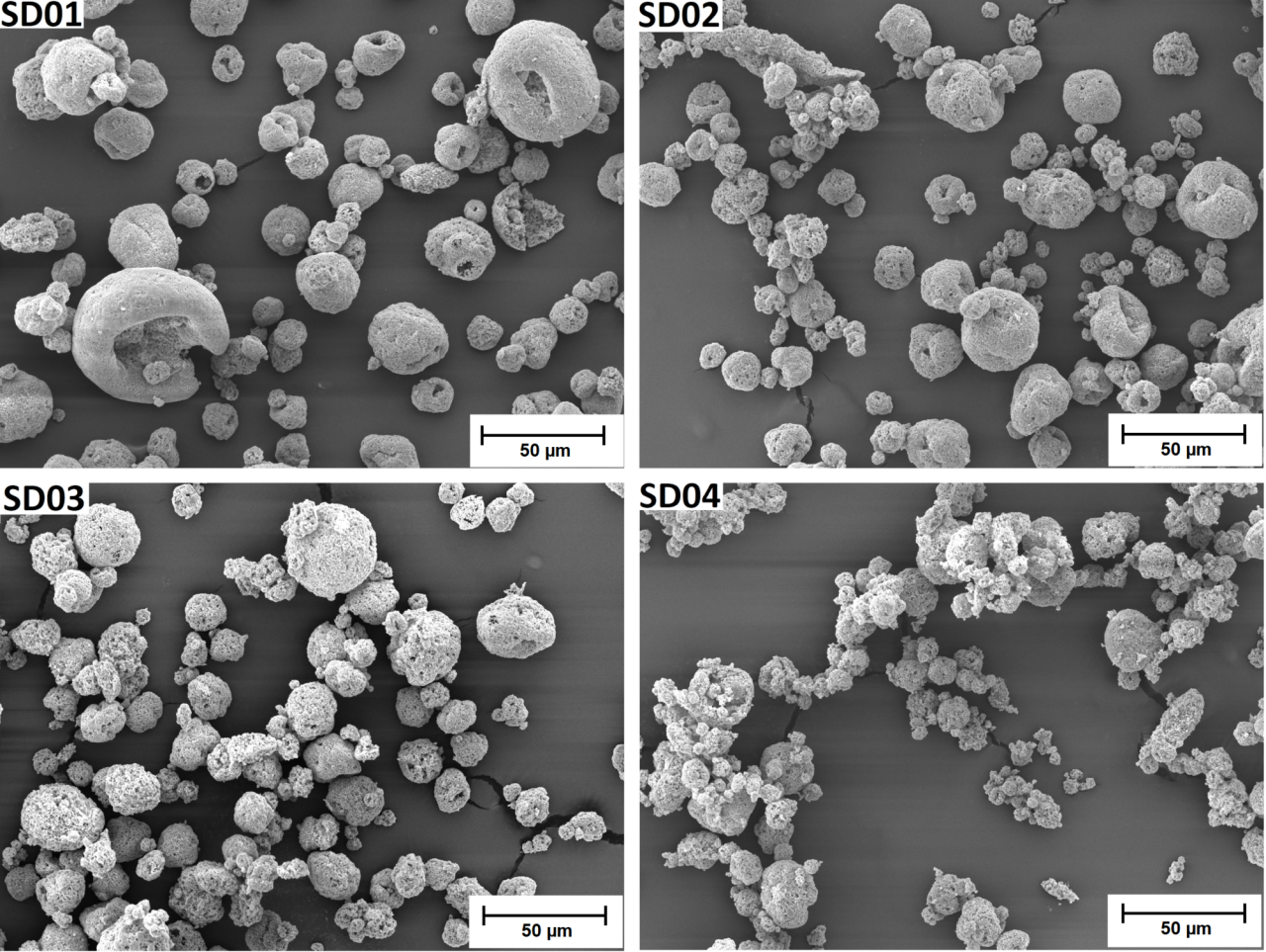
SD01
50 µm
SD02
50 µm
SD03
50 µm
SD04
50 µm

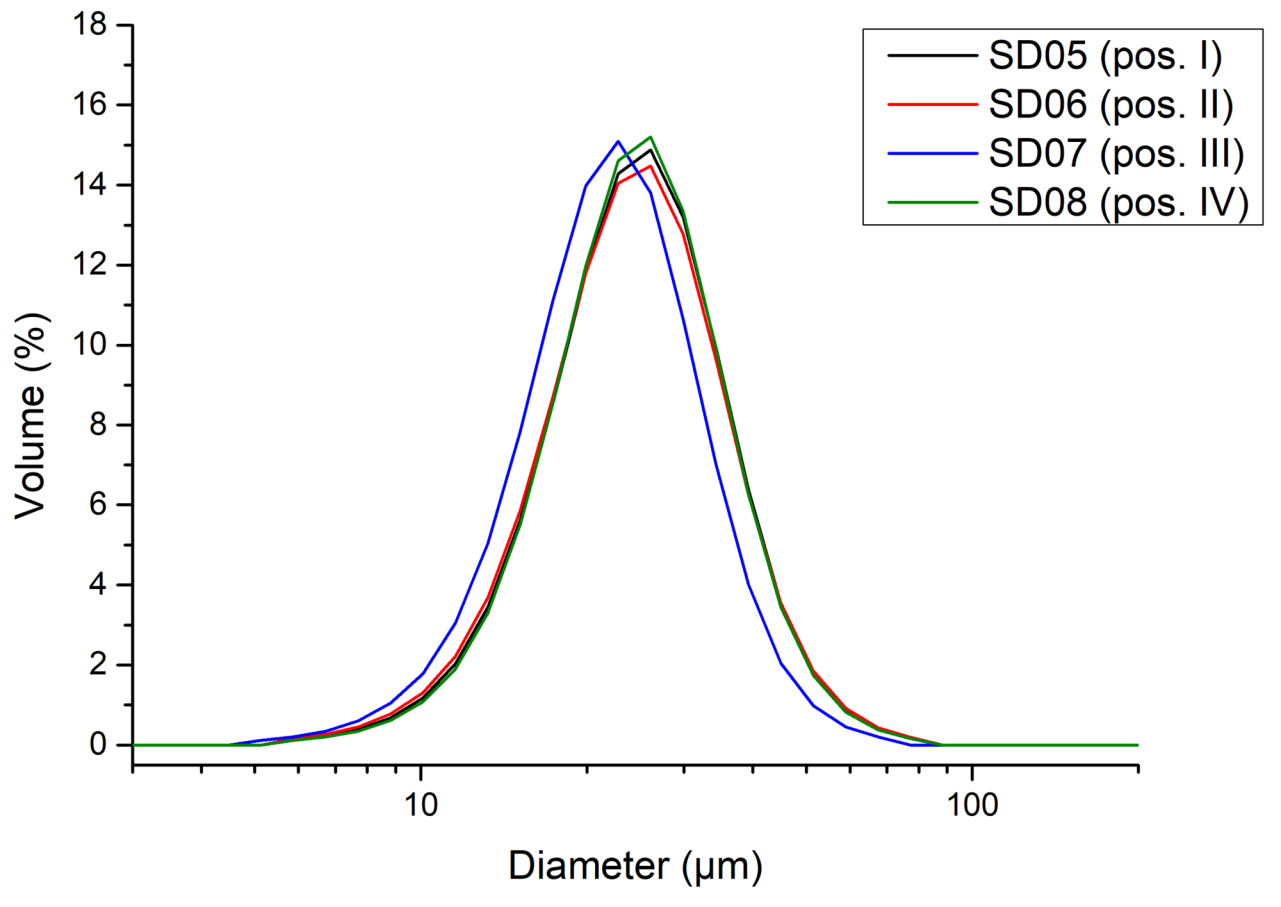
SD05 (pos. I)
SD06 (pos. II)
SD07 (pos. III)
SD08 (pos. IV)
Volume (%)
0
2
4
6
8
10
12
14
16
18
10
100
Diameter (µm)

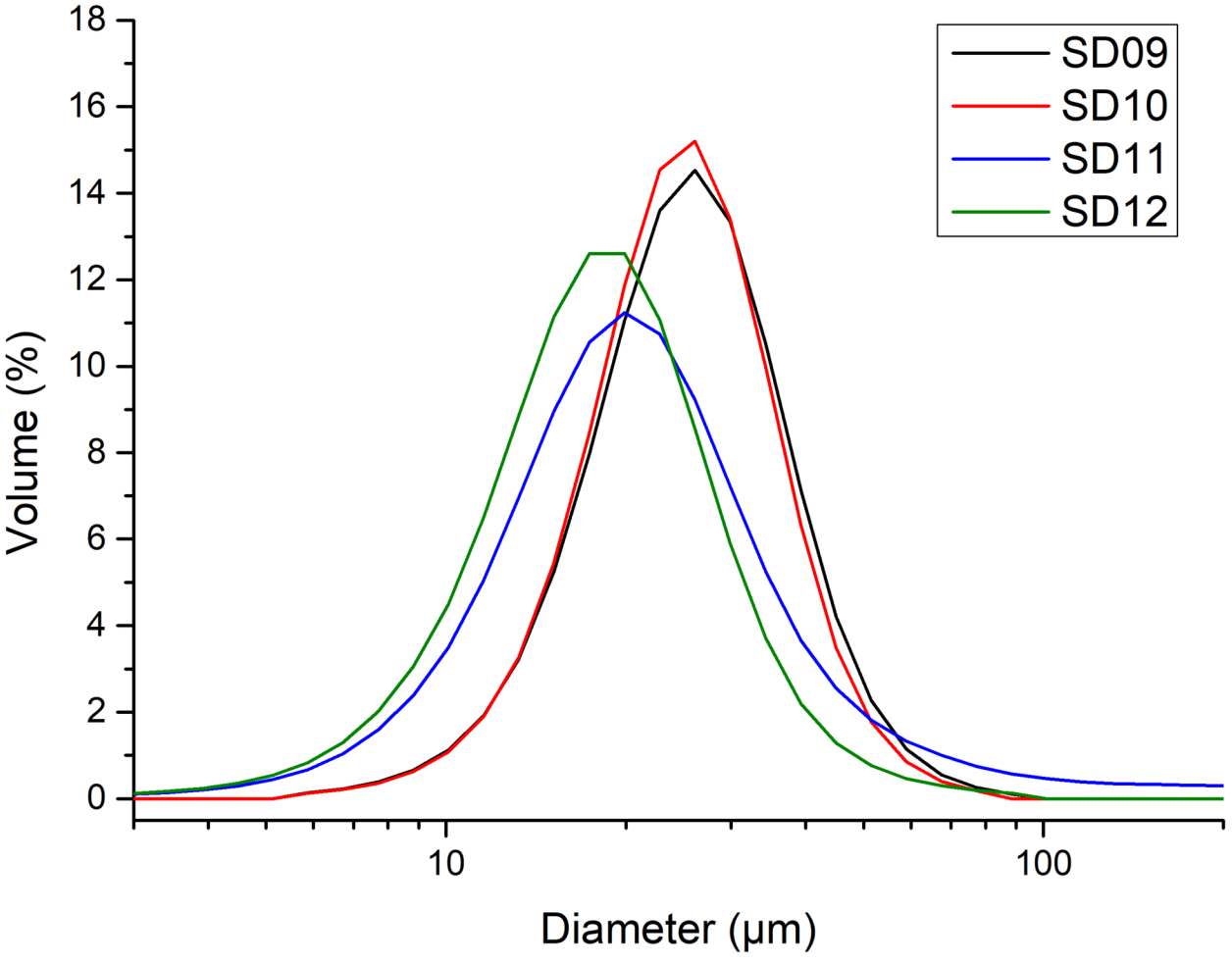
SD09
SD10
SD11
SD12
Volume (%)
Diameter (μm)
0
2
4
6
8
10
12
14
16
18
10
100

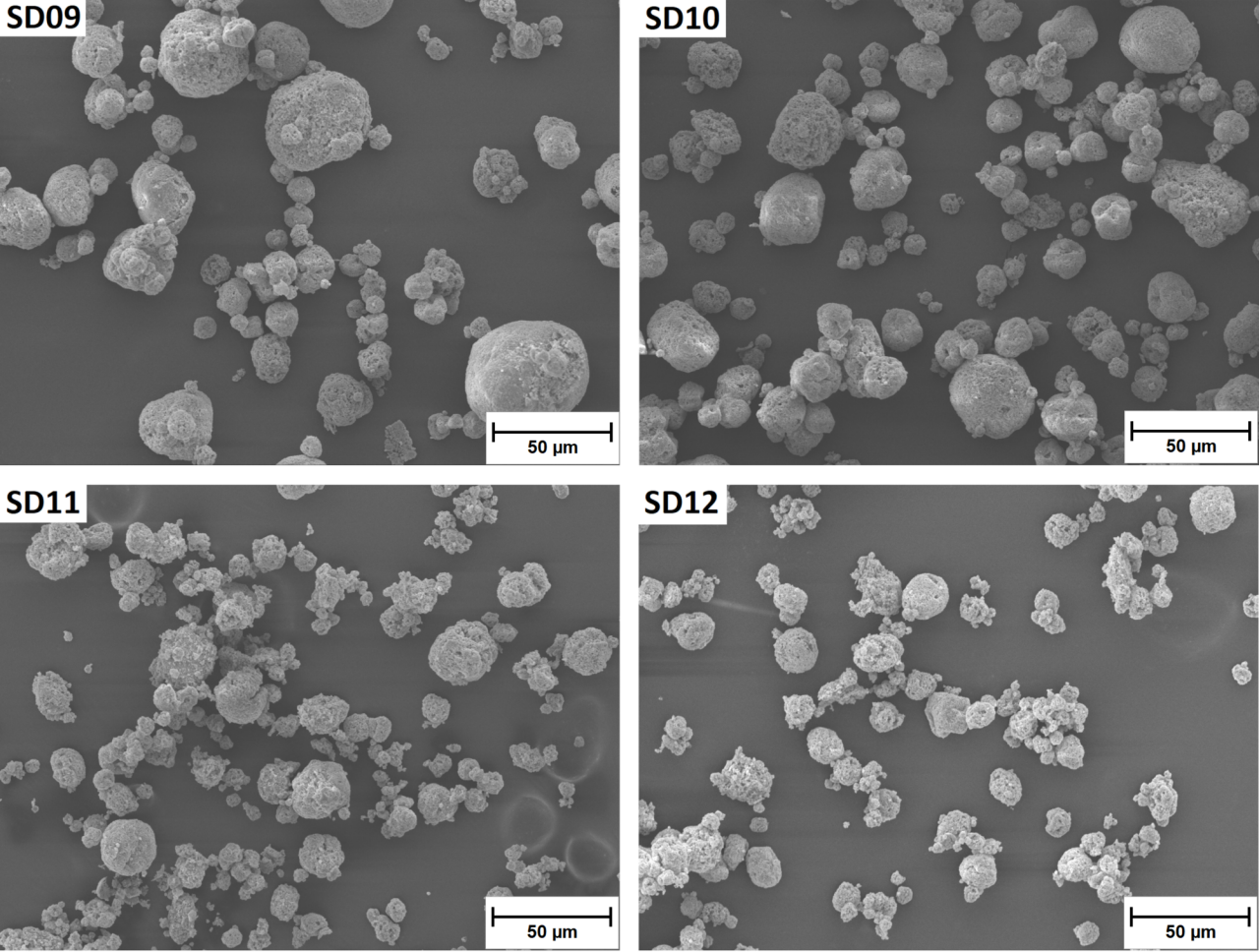
SD09
50 µm
SD10
50 µm
SD11
50 µm
SD12
50 µm

Table 1 – Compositions of spray-drying HA aqueous suspensions.

Sample	Hydroxyapatite (wt%)	Methylcellulose (wt%)	Deionized water (wt%)
SD01	20.00	3.20	76.80
SD02	20.16	2.42	77.42
SD03	20.32	1.63	78.05
SD04	20.49	0.82	78.69

Table 2 – Rheological values obtained from the Herschel–Bulkley model and respective D10, D50, D90 and ratios measures for HA suspensions.

Sample	Yield Stress (Pa)	Viscosity (Pa·s)	Rate index	D10 (µm)	D50 (µm)	D90 (µm)	(D90-D10)/D50 (µm)
SD01	8.47	1.70	0.67	2.18	5.43	55.65	23.08
SD02	8.56	1.07	0.66	2.13	5.88	46.99	19.32
SD03	5.91	0.51	0.65	2.24	5.10	12.42	3.26
SD04	5.92	0.18	0.70	2.22	4.29	8.36	1.83

Table 3 – Factorial design parameters and values and respective D10, D50, D90 mean size and size ratios, after heat treatment at 1000 °C for 1 h. The (-) signal represents lower and (+) higher values of the two levels factorial design.

Run	Sample	Atomization pressure (mmHg)	Slurry feed (mL min^{-1})	D10 (µm)	D50 (µm)	D90 (µm)	(D90-D10)/D50 (µm)
1	SD09	45 (-)	21.00 (-)	13.92	23.67	38.15	1.04
2	SD10	45(-)	25.50 (+)	13.90	23.12	36.53	0.96
3	SD11	60 (+)	21.00 (-)	9.71	19.02	39.52	2.11
4	SD12	60 (+)	25.50 (+)	9.01	16.85	29.24	1.37

Table 4 – Factorial design parameters and values and respective D10, D50, D90 mean size and

Sample	Analyzed responses			Individual desirability			Global desirability
	D50 (µm)	(D90-D10)/D50 (µm)	Particle morphology	D50	(D90-D10)/D50	Particle morphology	
SD09	23.67	1.04	4	86.70%	97.33%	75.00%	85.86%
SD10	23.12	0.96	4	81.20%	100.00%	75.00%	84.76%
SD11	19.02	2.11	3	40.20%	26.00%	50.00%	37.39%
SD12	16.85	1.37	3	18.50%	75.33%	50.00%	41.15%

Suspension Preparation

Hydroxyapatite
Methylcellulose
Deionized water

Particle size distribution
Rheological behavior

Spray Drying Process Using Factorial Design Experiment

Powder for selective laser sintering

Particle size distribution
Morphology

Particle's Characteristics